Journal of Sound and Vibration (1998) **209**(2), 203–222

ACOUSTIC–VORTICITY WAVES IN SWIRLING FLOWS

V. V. GOLUBEV AND H. M. ATASSI

University of Notre Dame, Notre Dame, IN 46556, *U.S.A.*

(*Received* 14 *June* 1996, *and in final form* 21 *March* 1997)

The propagation of small disturbances in an annular duct with a mean vortical swirling flow is studied. The disturbance velocity is split into a nearly-convected part and a nearly-sonic part, obeying weakly coupled equations. A normal mode analysis shows that the eigenvalues are segregated into a finite number of propagating pressure-dominated nearly-sonic waves and a cluster of infinite number of vorticity-dominated nearly-convected modes. A generalized gust can then be identified with the vorticity-dominated nearly-convected eigensolutions. The nearly-convected eigenvalues form two branches on either side of a critical layer which corresponds to purely convected modes. An asymptotic analysis is used to investigate the stability of the nearly-convected eigensolutions in the vicinity of the critical layer.

1. INTRODUCTION

The propagation of small disturbances in axial flow tubomachines and their interaction with a blade row have been extensively investigated in view of their relevance to noise generation and aeroelastic instabilities such as flutter and forced vibration. In modelling such flows, the disturbances are usually imposed upstream on a uniform mean flow. This brings about a significant simplification making it possible to split the flow disturbances upstream into distinct acoustic, entropic and vortical modes obeying separate equations [1]. These various modes may couple as the flow moves downstream and interacts with a blade row. This model is adequate for inlet distortions interacting with a blade row. However, for disturbances developing and propagating behind a rotor stage, the flow has a significant mean swirl which may strongly affect the nature and propagation of the disturbances as well as the unsteady forces and noise resulting from their interaction with a downstream blade row.

Kerrebrock [2] analyzed the effect of a mean flow swirl on the propagation of small disturbances in a duct. He pointed out that disturbances of flows with strong rotation will generate imbalanced centrifugal and Coriolis forces which will couple the vorticity, entropy and pressure modes. Kerrebrock also carried out a normal mode analysis to quantify the effects of mean flow swirl. His analysis indicates that shear disturbances are not purely convected by the mean flow but rather exhibit an oscillatory behavior. Such *nearly-convected* disturbances carry a weak pressure component with them.

The objective of the present paper is to revisit the problem of propagation of small disturbances in swirling flows as a step toward formulating and developing an aerodynamic/aeroacoustic model for thier propagation and interaction with a downstream blade row. To this end, Kerrebrock's important conclusion that shear disturbances are nearly-convected and carry only a weak pressure component is used to split the velocity

0022–460X/98/020203 + 20 $25.00/0/sv971049

field into a nearly-convected part and a nearly-sonic part, obeying weakly coupled equations. This splitting has the advantage of elucidating the physical phenomena which involve two types of waves, vorticity-dominated and pressure-dominated, and thus paves the way for generalizing the classical definition of a gust in vortical swirling flow. The present analysis gives a *complete* description of the system of waves developing in the fluid. Certain cases may be omitted if the treatment were only confined to a normal mode analysis. For example in the case of a free vortex flow, Kerrebrock's analysis shows that all shear waves would be unstable and would grow exponentially. By contrast, the present analysis shows that in the case of a potential swirl the velocity of the disturbances remains finite, the pressure associated with them decays, while the vorticity increases linearly as they propagate along the axis of the machine. Similar results were also obtained by Wundrow [3]. The failure of normal mode analysis to predict the correct behavior of the vortical waves results from an incorrect limiting process of a singular eigenvalue equation.

As in Kerrebrock's analysis, the mean flow is represented as a combination of a uniform axial flow, a solid body rotation, and a free vortex. This mean flow model defines the swirl in terms of two parameters representing the angular velocity and the strength of the axial vortex and gives a good approximation of turbomachinery flows [4]. In a previous paper [5], the authors considered the propagation of acoustic waves in an annular duct with mean potential swirling flow. In this case, the acoustic modes can be independent of the vortical modes. Nonetheless, a normal mode analysis leads to a non-Sturm–Liouville eigenvalue problem (not self-adjoint). The results show that the refraction effect of the mean swirl changes the modal phase speeds and thus modifies the cut-on frequency due a Doppler shift. Thus, modes propagating opposite to the swirling motion have a smaller cut-on frequency. Similar results are usually found in problems associated with the propagation of acoustic waves in ducts with shear boundary layers next to the wall. The corresponding eigenvalue problem is also not self-adjoint and it is not possible for such boundary value problems to reach conclusions about orthogonality and completeness of the set of eigenfunctions. It is worth noting that the refraction effects resulting from the wall shear layer can also significantly affect the propagation of sound waves in ducts. These effects have been extensively studied in the 70s, and a detailed review was given by Nayfeh *et al*. [6].

The mathematical formulation leads to a system of equations for the normal modes. The resulting eigenvalue problem, which is not self-adjoint, is solved numerically using a pseudo-spectral technique for accuracy. As a result of the vorticity in the mean flow, a *critical layer* appears in the flow where the wave speed equals the fluid speed. As one approaches the critical layer, the accuracy of the numerical scheme is not sufficient to resolve the structure of the flow. An asymptotic analysis is then employed to properly and accurately determine the eigensolutions.

2. FORMULATION

The propagation of small-amplitude unsteady disturbances in an annular inviscid, non-heat-conducting, swirling flow (see Figure 1) is considered. The total velocity field is assumed to be

$$\vec{V}(\vec{x}, t) = \vec{U}(\vec{x}) + \vec{u}(\vec{x}, t), \tag{1}$$

where $\vec{U}(\vec{x})$ is the mean flow velocity and $\vec{u}(\vec{x}, t)$ represents the disturbance velocity such that $|\vec{u}(\vec{x}, t) \ll |\vec{U}(\vec{x})|$. The pressure and density of the fluid can also be written as

$$p(\vec{x}, t) = p_0(\vec{x}) + p'(\vec{x}, t), \qquad \rho(\vec{x}, t) = p_0(\vec{x}) + \rho'(\vec{x}, t), \tag{2}$$

where the time dependent perturbation quantities are assumed to be much smaller than those of the mean flow, and governed by the linearized Euler equations.

The mean flow is assumed to have an axial velocity U_0 with rigid body rotation and a free axial vortex. Thus, one can write

$$\vec{U}(\vec{x}) = U_0 \hat{e}_x + (\Omega r + \Gamma/r)\hat{e}_\theta,$$

where Ω and Γ are two constants representing the angular velocity of the solid body rotation and the strength of the axial vortex circulation, respectively; r is the radial distance, $\hat{e}_x$ and $\hat{e}_\theta$ represent unit vectors in the axial and circumferential directions, respectively.

The disturbance velocity is now decomposed into potential and rotational parts,

$$\vec{u} = \nabla\phi + \vec{u}^{(R)}. \tag{3}$$

Without loss of generality, one assumes that

$$p' = -\rho_0 \, \mathrm{D}_0\phi/\mathrm{D}t, \tag{4}$$

and as a result, the linearized Euler equations are reduced to the following two *coupled* equations [8]:

$$\frac{\mathrm{D}_0\vec{u}^{(R)}}{\mathrm{D}t} + (\vec{u}^{(R)} \cdot \nabla)\vec{U} = -\vec{\zeta} \times \nabla\phi, \qquad \mathscr{L}\phi = (1/\rho_0)\nabla \cdot (\rho_0 \vec{u}^{(R)}), \tag{5, 6}$$

where the mean flow vorticity is $\vec{\zeta} = 2\Omega\hat{e}_x$, ρ_0 is the mean flow density, $\mathrm{D}_0/\mathrm{D}t$ is the convected derivative

$$\mathrm{D}_0/\mathrm{D}t = \partial/\partial t + U_0 \, \partial/\partial x + (\Gamma/r^2 + \Omega) \, \partial/\partial\theta, \tag{7}$$

and $\mathscr{L}$ is the convected wave operator defined as

$$\mathscr{L} \equiv (\mathrm{D}_0/\mathrm{D}t)\,(1/c_0^2)\,(\mathrm{D}_0/\mathrm{D}t) - (1/\rho_0)\nabla \cdot (\rho_0 \nabla), \tag{8}$$

where c_0 is the mean flow speed of sound. Assuming rigid duct walls, the boundary conditions at the hub and tip radii r_h and r_t are

$$\partial\phi/\partial r + u_r^{(R)} = 0, \tag{9}$$

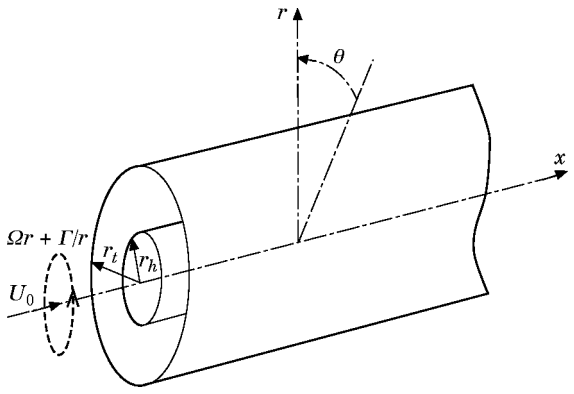

Figure 1. Swirling mean flow in an annular duct.

where $u_r^{(R)}$ is the radial component of $\vec{u}^{(R)}$. Note that the governing equations (4), (5), and (6) are valid for any non-axisymmetric mean flow. The coupling between the vortical and potential modes in equations (5, 6) shows that, due to the non-uniformity of the mean flow, an inlet vortical disturbance will always induce an unsteady "hydrodynamic" pressure field. However, equation (5) suggests that, *if* the mean flow is irrotational, an incident potential disturbance will not create a vortical perturbation of the velocity field. Thus, the solution to the coupled equations (5) and (6) depends on the upstream condition of the unsteady flow. In the eigenmode analysis of an unsteady vortical swirling flow presented below, one assumes incident potential perturbations of the flow. Thus, the vortical disturbances can only be initiated through the coupling in equations (5) and (6) which occurs for rotational mean flows.

2.1. NORMAL MODE EXPANSION

The normal mode analysis is used to obtain the spectrum of propagating and evanescent acoustic–vorticity modes of equations (5) and (6). To this end, the following Fourier expansion is assumed:

$$\{u_x^{(R)}, u_r^{(R)}, u_\theta^{(R)}, \phi\}(x, r, \theta; t) = \int_{-\infty}^{\infty} \sum_{m=-\infty}^{\infty} \sum_{n=1}^{\infty} \{X_{mn}(r), R_{mn}(r), T_{mn}(r), \varphi_{mn}(r)\} \times e^{i(-\omega t + m\theta + k_{mn} x)}\, d\omega, \tag{10}$$

where m and n are integer modal numbers characterizing the circumferential and radial eigenmodes, respectively. Due to the linear character of the problem, each Fourier component of the solution vector can be considered separately. Using equation (4), the pressure modes are given by

$$p'_{mn}(r) = -i\rho_0(r)\varphi_{mn}(r)\Lambda_{mn}, \tag{11}$$

where Λ_{mn} is an eigenvalue of the convected operator D_0/Dt, defined by

$$\Lambda_{mn} = k_{mn} U_0 - \omega + m(\Omega + \Gamma/r^2). \tag{12}$$

Note that Λ_{mn} is a function of radius which appears as a parameter in D_0/Dt.

The coupled system of equations (5) and (6) can now be represented in terms of normal modes as

$$\Lambda_{mn} X_{mn}(r) = 0, \qquad \Lambda_{mn} R_{mn}(r) + 2iT_{mn}(r)(\Omega + \Gamma/r^2) - (2\Omega m/r)\varphi_{mn}(r) = 0,$$

$$i\Lambda_{mn} T_{mn}(r) + 2\Omega R_{mn}(r) + 2\Omega\, d\varphi_{mn}(r)/dr = 0,$$

$$\frac{d^2\varphi_{mn}(r)}{dr^2} + \left(\frac{1}{r} + \frac{d \ln \rho_0}{dr}\right)\frac{d\varphi_{mn}(r)}{dr} + \left(\frac{\Lambda_{mn}^2}{c_0^2} - k_{mn}^2 - \frac{m^2}{r^2}\right)\varphi_{mn}(r)$$

$$+ \left(\frac{1}{r} + \frac{d \ln \rho_0}{dr}\right)\frac{R_{mn}(r)}{r} + \frac{dR_{mn}(r)}{d\, r} + \frac{im}{r} T_{mn}(r) + ik_{mn} X_{mn}(r) = 0. \tag{13}$$

If one considers only incident potential perturbations then the uncoupled axial component of the vortical velocity $X_{mn}(r) = 0$. One assumes a duct with rigid walls, and therefore the boundary conditions for equations (13) are

$$R_{mn}(r) + d\varphi_{mn}(r)/dr = 0 \tag{14}$$

at hub and tip radii $r = r_h$ and $r = r_t$. The properties of numerical solutions of the eigenvalue problem (13, 14) are investigated for different kinds of the mean swirl. The eigenvalues k_{mn} represent allowed axial wavenumbers of the acoustic–vorticity modes.

2.2. CRITICAL LAYER

The eigenvalues k_{mn} corresponding to $\Lambda_{mn} = 0$ represent the purely convected modes. It will be shown now that, in the general case of a vortical mean swirl, the boundary value problem defined by equations (13, 14) has a *critical layer* corresponding to $\Lambda_{mn} \to 0$. First, the following transformation is introduced:

$$\psi_{mn}(r) = \varphi_{mn}(r)\,[r^2\Lambda_{mn}]^{m\Omega/(-\omega + U_0 k + m\Omega)}, \tag{15}$$

and then the eigenfunctions $R_{mn}(r)$ and $T_{mn}(r)$ are eliminated from equations (13). The boundary value problem reduces to a single equation:

$$\psi''_{mn}\left\{\frac{\Lambda_{mn}^2}{D(\Lambda_{mn})}\right\} + \psi'_{mn}\left\{\left(\frac{1}{r} + \frac{\mathrm{d}(\ln \rho_0)}{\mathrm{d}r}\right)\frac{\Lambda_{mn}^2}{D(\Lambda_{mn})}\right.$$

$$\left. + \frac{4\Lambda_{mn}\Omega[m\Lambda_{mn}^2 r^2 + 2\Lambda_{mn}\Gamma - 4mr^2(\Omega + \Gamma/r^2)^2]}{r^3 D^2(\Lambda_{mn})}\right\} + \psi_{mn}\left\{\frac{m^2}{r^2} + k_{mn}^2 - \frac{\Lambda_{mn}^2}{c_0^2}\right\} = 0 \tag{16}$$

with boundary conditions

$$\mathrm{d}\psi_{mn}(r)/\mathrm{d}r = 0 \tag{17}$$

at $r = r_h$ and $r = r_t$, where $D(\Lambda_{mn}) = 4\Omega(\Omega + \Gamma/r^2) - \Lambda_{mn}^2$. It is important to point out that the eigenvalue k_{mn} appears in a non-linear way in all the coefficients of equation (16), and as a result, the boundary value problem (16, 17) is not a Sturm–Liouville problem.

Note that once this problem is solved and the potential eigenfunction $\varphi_{mn}(r)$ is recovered from equation (15), the azimuthal and radial vortical velocity modes are immediately deduced from equation (13):

$$T_{mn}(r) = -[4\mathrm{i}m\Omega^2/rD(\Lambda_{mn})]\varphi_{mn}(r) - [2\mathrm{i}\Omega\Lambda_{mn}/D(\Lambda_{mn})]\,\mathrm{d}\varphi_{mn}(r)/\mathrm{d}r,$$

$$R_{mn}(r) = -[2m\Omega\Lambda_{mn}/rD(\Lambda_{mn})]\varphi_{mn}(r) - [4\Omega(\Omega + \Gamma/r^2)/D(\Lambda_{mn})]\,\mathrm{d}\varphi_{mn}(r)/\mathrm{d}r. \tag{18}$$

Solution of equation (16) may possess a singular critical layer corresponding to a purely convected eigenmode with $\Lambda_{mn} = 0$. If $\Gamma \neq 0$, $\Omega \neq 0$ and $m \neq 0$, this layer extends for $\tilde{\omega}_m(r_h)U_0 \leqslant k_{mm} \leqslant \tilde{\omega}_m(r_t)/U_0$ or $\tilde{\omega}_m(r_t)/U_0 \leqslant k_{mm} \leqslant \tilde{\omega}(r_h)$ depending on the sign of m. In where $\tilde{\omega}_m = \omega - m(\Omega + \Gamma/r^2)$. In this case, an asymptotic behavior of the potential solution at the critical layer can be obtained directly from equation (16) for a range of circumferential modal numbers. Then, if it can be shown that for certain m the solution is singular at $\Lambda_{mn} = 0$, it may indicate that solution of the corresponding initial value problem develops an instability wave asymptotically represented by the singular eigenmodes.

By assuming that the convected solution is sought for a certain $r = r_c$, and introducing Λ_{mn} as a new variable $\xi(r)$ so that $\xi \to 0$ for $r \to r_c$, equation (16) reduces to leading to

$$\xi^2\psi''_{mn} + a_1\xi\psi'_{nm} + a_2\psi_{mn} = 0, \tag{19}$$

where the derivatives are now taken with respect to ξ, real constants a_1 and a_2 are estimated at $r = r_c$ and $k_{mn} = k_c$,

$$a_1 = 2(\Omega r_c^2 + \Gamma)/\Gamma, \qquad a_2 = \Omega r_c^2(\Omega r_c^2 + \Gamma)(m^2 + r_c^2 k_c^2)/m^2\Gamma^2, \tag{20}$$

Thus $\xi = 0$ is a regular singular point, and at least one non-trivial solution of equation (19) exists of the form

$$\psi_{mn}(\xi) = \xi^s \sum_{l=0}^{\infty} A_l \xi^l \tag{21}$$

which can be regular or irregular near $\xi = 0$ depending on the value of exponent s. The latter is determined from the indicial equation

$$s^2 + s(a_1 - 1) + a_2 = 0 \tag{22}$$

which gives

$$s_{1,2} = -(\Omega r_c^2/\Gamma + 1/2) \pm [1/4 - \Omega r_c^4(\Omega r_c^2 + \Gamma)k_c^2/m^2\Gamma^2]^{1/2}. \tag{23}$$

For a convected mode such that $|m| > 2k_c r_c^2[\Omega(\Omega r_c^2 + \Gamma)]^{1/2}/\Gamma$, the exponents are real and equal to $s_{1,2} = -(\Omega r_c^2/\Gamma + 1/2) \pm \beta$, where $0 < \beta < 1/2$ is a real constant. In view of transformation (15) for $\xi \to 0$, the potential eigenfunction $\varphi_{mn}(\xi) = (r_c^2\xi)^{\Omega r_c^2/\Gamma}\psi_{mn}(\xi)$ assumes two linearly independent real solutions singular at $\xi = 0$, of the form

$$\varphi_{mn}^{(1,2)}(\xi) = \xi^{-1/2 \pm \beta} \sum_{l=0}^{\infty} A_l \xi^l. \tag{24}$$

On the other hand, if $|m| < 2k_c r_c^2[\Omega(\Omega r_c^2 + \Gamma)]^{1/2}/\Gamma$, the indicial equation gives two complex conjugate numbers $s_{1,2} = -(\Omega r_c^2/\Gamma + 1/2) \pm i\beta$ ($\beta > 0$) and hence two oscillatory complex eigenfunctions

$$\varphi_{mn}(\xi) + \xi^{-1/2} \exp\{\pm i\beta \log \xi\} \sum_{l=0}^{\infty} A_l \xi^l. \tag{25}$$

In addition to singularity at $\xi = 0$, the frequency of modal oscillations also becomes infinite at this point. Note that more spinning modes will exhibit such behavior as the portion of rigid body rotation is increased in the mean swirl.

From equations (18), the total circumferential and radial velocity modes behave at the critical layer like

$$T_{mn}(r) + im\varphi_{mn}(r)/r = im\Gamma(\varphi_{mn}(\xi) + \xi\, d\varphi_{mn}(\xi)/d\xi)/r_c(\Omega r_c^2 + \Gamma) \tag{26}$$

and

$$R_{mn}(r) + d\varphi_{mn}(r)/dr = -mr_c\xi\varphi_{mn}(\xi)/2(\Omega r_c^2 + \Gamma), \tag{27}$$

respectively. The axial velocity mode is just $ik_c\varphi_{mn}(\xi)$. Note that as in Kerrebrock's analysis, the radial component vanishes as $\xi \to 0$. However, the axial and circumferential perturbation velocities are singular at the critical layer.

The convected pressure mode is $i\rho_0(r_c)\xi\varphi_{mn}(\xi)$, and thus also vanishes at the critical point for any m. The pressure gradient is, however, singular since, as it would be expected, it must balance the singular velocities at the critical layer.

It will be shown below that a set of discrete *nearly-convected* eigenvalues surrrounds the convected region. Examination of equation (16) indicates that near the convected region,

eigensolutions will exist only when both coefficients of ψ''_{mn} and ψ_{mn} are positive. This implies that $D(\Lambda_{mn}) \geqslant 0$, or

$$-2\sqrt{\Omega(\Omega + \Gamma/r_h^2)} \leqslant \Lambda_{mn} \leqslant 2\sqrt{\Omega(\Omega + \Gamma/r_t^2)}. \tag{28}$$

One may expect the pressure associated with these nearly-convected eigenmodes to become more significant as the eigenvalues move away from the convected critical layer. Such modes thus may be particularly important in the formulation of the inflow/outflow conditions. In order to carefully investigate the behavior of nearly-convected solution, the numerical normal mode analysis of equations (13) presented below will be complemented later by a multiple-scale eigenvalue analysis of equation (16) in the vicinity of the critical layer.

2.3. POTENTIAL SWIRLING FLOW

In the case of a potential swirl, the mean flow is represented as a combination of a uniform flow and a free vortex swirl, $\vec{U} = U_0\hat{e}_x + (\Gamma/r)\hat{e}_\theta$. This problem was investigated in reference [5]. Equations (13) suggest that the convected modes are uncoupled from the pressure modes. This corresponds to the homogeneous solution of equation (5) and suggests the following modal expansion:

$$\{u_x^{(R)}, u_r^{(R)}, u_\theta^{(R)}, \phi\}(x, r, \theta; t) = \int_{-\infty}^{\infty} \sum_{m=-\infty}^{\infty} \sum_{n=1}^{\infty} \{X_{mn}(r), R_{mn}(r) + \frac{2\Gamma}{r^2 U_0} x T_{mn}(r), T_{mn}(r), \varphi_{mn}(r)\} \, e^{i(-\omega t + m\theta + k_{mn}x)} \, d\omega. \tag{29}$$

This implies the existence of a secular term which amplifies the radial vortical velocity. Therefore such modes will grow algebraically in a duct with potential mean swirl. Note that in reference [8] it was shown that for an initial-value problem, this secular term is cancelled by a similar term of the potential velocity arising from the inhomogeneous wave equation (6). It was also shown that the pressure caused by these modes acting as a source in equation (6) will vanish at large distances. Hence, only pressure-less convected vorticity modes will propagate far downstream in a duct.

On the other hand, the pressure modes associated with the potential velocity will correspond to a homogeneous solution of equation (6). Thus, the pressure waves will propagate exactly as sound waves in the non-uniform medium of the potential swirling flow, i.e., the wave speed will be equal to the speed of sound in a local frame of reference moving with the local mean flow. Note that this is not the case for a vortical swirling mean flow, where the coupling between vortical and potential modes will force the discrete pressure modes to propagate with phase speeds different from the local speed of sound.

The corresponding eigenvalue problem for discrete sound pressure modes is then reduced [5] to solving a homogeneous equation:

$$\mathscr{L}\phi = 0. \tag{30}$$

In equation (16), one has $\Omega = 0$, $D(\Lambda_{mn}) = -\Lambda_{mn}^2$, and $\psi_{mn}(r) = \varphi_{mn}(r)$, which reduces the eigenvalue problem to

$$\left\{\frac{d^2}{dr^2} + \left(\frac{1}{r} + \frac{d(\ln \rho_0)}{dr}\right)\frac{d}{dr} + \left(\frac{\Lambda_{mn}^2}{c_0^2} - k_{mn}^2 - \frac{m^2}{r^2}\right)\right\}\varphi_{mn}(r) = 0, \tag{31}$$

with $\partial\varphi_{mn}(r)/\partial r = 0$ at $r = r_h$ and $r = r_t$. Note that this boundary value problem does not have a critical layer as Λ_{mn} is no loner a singular parameter of the problem. However, it still appears non-linearly in the eigenvalue equation as a result of refraction of the sound waves by the mean flow. The eigensolution of equation (32) was analyzed in detail in reference [5].

2.4. VORTICAL SWIRLING FLOW

In the general case, one describes the mean flow as a combination of an axial flow, rigid body rotation, and a free vortex: $\vec{U} = U_0\hat{e}_x + (\Omega r + \Gamma/r)\hat{e}_\theta$. Note that Λ_{mn} is a non-linear parameter of the eigensystem (13). To solve the problem numerically, a new variable $\eta_{mn}(r) = k_{mn}\beta_0^2\varphi_{mn}(r)$ ($\beta_0^2 = 1 - (U_0/c_0)^2$), is introduced, which brings the eigensystem (13) to the following standard form:

$$\begin{bmatrix} 0 & 1/\beta_0^2 & 0 & 0 \\ \mathscr{R} & -\dfrac{2\tilde{\omega}_m U_0}{c_0^2\beta_0^2} & \left(\dfrac{\mathrm{d}}{\mathrm{d}r} + \dfrac{1}{r} + \dfrac{\mathrm{d}(\ln\rho_0)}{\mathrm{d}r}\right) & \dfrac{m}{r} \\ \dfrac{2m\Omega}{rU_0} & 0 & \dfrac{\tilde{\omega}_m}{U_0} & -\dfrac{2(\Omega + \Gamma/r^2)}{U_0} \\ -\dfrac{2\Omega}{U_0}\dfrac{\mathrm{d}}{\mathrm{d}r} & 0 & -\dfrac{2\Omega}{U_0} & \dfrac{\tilde{\omega}_m}{U_0} \end{bmatrix} \begin{bmatrix} \varphi_{mn} \\ \eta_{mn} \\ R_{mn} \\ \mathrm{i}T_{mn} \end{bmatrix} = k_{mn} \begin{bmatrix} \varphi_{mn} \\ \eta_{mn} \\ R_{mn} \\ \mathrm{i}T_{mn} \end{bmatrix}, \tag{32}$$

where the differential operator

$$\mathscr{R} = \frac{\mathrm{d}^2}{\mathrm{d}r^2} + \left(\frac{1}{r} + \frac{\mathrm{d}(\ln\rho_0)}{\mathrm{d}r}\right)\frac{\mathrm{d}}{\mathrm{d}r} + \left(\frac{\tilde{\omega}_m^2}{c_0^2} - \frac{m^2}{r^2}\right),$$

and boundary conditions are defined by equation (14). Equation (32), shows that the potential and vortical modes are coupled and suggests that the eigenmode will represent coupled acoustic–vorticity modes. The eigensystem can be solved numerically, and in the following discussion the focus will be on the methods of solution applied to this system.

3. NUMERICAL SOLUTION

The eigensystem (32) was solved numerically using two computational methods: a finite difference technique, and a pseudo-spectral method [9]. Both of them eventually reduced the problem to solving an algebraic eigensystem, which was then implemented by a shifted QR algorithm (e.g., reference [10]). The finite difference scheme used a straightforward fourth order approximation of differential oeprators in equation (33), with boundary conditions (14) incorporated in the system at the end points of the computational domain. If N is the number of grid points used in the numerical discretization of the domain $r_h < r < r_t$, then one obtains $4N$ different eigenvalues $(k_{m,1}, k_{m,2}, \ldots, k_{m,4N})$ for a given frequency ω and circumferential modal number m.

However, the accuracy of the finite difference scheme was not sufficient to resolve the *nearly-convected* eigensolutions in the vicinity of a critical layer $\Lambda_{mn} = 0$. The *pseudo-spectral* method yields more accurate results, though, as will be seen in the

following section, there always remains a region close to the critical layer where asymptotic analysis is needed. The *pseudo-spectral* method is based on the Chebyshev expansion method with exponential convergence, and thus is capable of accurately resolving thin layers of steep changes such as critical layers [9]. In addition, the pseudo-spectral method employs the convenience of calculating derivatives and integrals from Chebyshev expansions. With the collocation points selected as $x_l = \cos[\pi(l-1)/(N-1)]$ for $1 \leqslant l \leqslant N$, each eigenfunction of the system is represented as

$$f_l = \sum_{p=1}^{N} a_p \cos \frac{\pi(p-1)\,(l-1)}{N-1},$$

where a_p are coefficients of the spectral expansion. If one defines (in matrix form) $\mathbf{f} = (f_1, f_2, \ldots, f_N)^{\mathrm{T}}$, then the first and second derivative vectors are determined by

$$\mathbf{f}' = \mathbf{W}^{(1)}\mathbf{f}, \qquad \mathbf{f}'' = \mathbf{W}^{(2)}\mathbf{f}. \tag{34}$$

The matrices $\mathbf{W}^{(1)}$ and $\mathbf{W}^{(2)}$ can be easily calculated from the values of Chebyshev polynomials in the collocation points (see reference [9]). The eigensystem then can be rewritten:

$$\begin{bmatrix} 0 & (1/\beta_0^2)\delta_{jl} & 0 & 0 \\ E_{jl} & -\dfrac{2\tilde{\omega}_m U_0}{c_0^2\beta_0^2}\,\delta_{jl} & \dfrac{2}{\Delta}\,W_{jl}^{(1)} + \left(\dfrac{1}{r} + \dfrac{\mathrm{d}(\ln\rho_0)}{\mathrm{d}r}\right)\delta_{jl} & \dfrac{\mathrm{i}m}{r}\,\delta_{jl} \\ \dfrac{2m\Omega}{rU_0}\,\delta_{jl} & 0 & \dfrac{\tilde{\omega}_m}{U_0}\,\delta_{jl} & -\dfrac{2\mathrm{i}(\Omega + \Gamma/r^2)}{U_0}\,\delta_{jl} \\ -\dfrac{4}{\Delta}\dfrac{\Omega}{U_0}\,W_{jl}^{(1)} & 0 & -\dfrac{2\Omega}{U_0}\,\delta_{jl} & \dfrac{\mathrm{i}\tilde{\omega}_m}{U_0}\,\delta_{jl} \end{bmatrix} \times \begin{pmatrix} \varphi_{ml} \\ \eta_{ml} \\ R_{ml} \\ \mathrm{i}T_{ml} \end{pmatrix} = k_{ml} \begin{pmatrix} \varphi_{ml} \\ \eta_{ml} \\ R_{ml} \\ \mathrm{i}T_{ml} \end{pmatrix} \tag{34}$$

where $1 \leqslant l \leqslant N$, $1 \leqslant j \leqslant N$, δ_{jl} is a Kronecker symbol, $\Delta = r_t - r_h$, and matrix

$$E_{jl} = \frac{4}{\Delta^2}\,W_{jl}^{(2)} + \frac{2}{\Delta}\left(\frac{1}{r} + \frac{\mathrm{d}(\ln\rho_0)}{\mathrm{d}r}\right)W_{jl}^{(1)} + \left(\frac{\tilde{\omega}_m^2}{c_0^2} - \frac{m^2}{r^2}\right)\delta_{jl}.$$

The collocation points $-1 \leqslant x_l \leqslant 1$ are mapped to $r_l = x_l\Delta/2 + (r_t + r_h)/2$. The boundary conditions (14) are transformed to

$$(2/\Delta)W_{1l}^{(1)}\varphi_{ml} + R_{m1} = 0, \qquad r = r_h, \qquad (2/\Delta)W_{Nl}^{(1)}\varphi_{ml} + R_{mN} = 0, \qquad r = r_t,$$

where, as before, the repeated indices l mean summation over them. These conditions are incorporated in equation (35) at the end points of the domain.

Since the original eigenvalue problem (13, 14) is not of the Sturm–Liouville type, the eigenvalues of equation (13) are in general complex. The calculations reveal two families of discrete eigenvalues $k_{mn}^{(u,d)}$ corresponding (in a local frame of reference moving with a local mean flow) to upstream and downstream propagating "pressure-dominated" eigenmodes. In addition, in the case of rotational mean flows, there appears a family of discrete

nearly-convected eigenvalues corresponding to "vorticity-dominated" acoustic–vorticity modes. The meaning of the quoted terms will become clear from the following discussion.

The eigenvalues are arranged as follows. Those eigenvalues which are real and thus correspond to propagating acoustic–vorticity waves are first considered. The *evanescent* and *amplifying* modes are arranged according to the increasing imaginary parts of the eigenvalues. Finally, the nearly-convected roots corresponding to $\Lambda_{mn} \to 0$ can be identified for rotational mean flows. In the numerical calculations, some of these eigenvalues are associated with spurious solutions as one comes close enough to the singular critical layer. However, contrary to eigenvalues which correspond to physically meaningful nearly-convected modes, spurious eigenvalues change as the numerical discretization is changed, and thus can be easily recognized. In the following discussion of numerical results, the spurious roots are not shown in the presented figures.

4. RESULTS OF NUMERICAL ANALYSIS

In this section the spectrum of acoustic–vorticity eigenmodes resulting from the numerical eigenvalue analysis of equation (33) is considered. The effect of the mean flow on the propagation of the modes in the upstream and downstream directions is examined, as well as the behavior of the eigensolutions near the critical layers. The results are presented in terms of the double set of eigenvalues $k_{mn}^{(u,d)}$ for $m = 0, 2, \pm 5$ and $n = 1, \ldots, 15$. The modes with positive and negative m correrspond to non-axisymmetric waves rotating with or opposite to the mean swirl, respectively. Note that the eignemodes are normalized numerically so that the norm of a complete eigenvector of equation (35) is defined by

$$\|f\| = \sum_{j=1}^{4(N+1)} [|\mathrm{Re}\,(f_j)| + |\mathrm{Im}\,(f_j)|]h = 1, \tag{35}$$

where h is the discretization step.

For numerical calculations, one considers an annular duct with hub and tip radii $r_h = 4$ and $r_t = 6$, respectively. A non-dimensional frequency $\bar{\omega} = \omega r_m / \bar{c}_0$ is also introduced, where r_m is the mean radius of the annulus and $\bar{c}_0$ is the stagnation speed of sound. The results are presented for $\bar{\omega} = 8$, for an axial flow Mach number $M_0 = 0{\cdot}3$. The total Mach number of the swirling flow components (specified at the mean radius) is fixed for $M_s = 0{\cdot}3$, but the nature of the swirl may vary.

The case of a potential swirling flow was considered in detail in reference [5], where the accuracy of the finite difference numerical scheme was also examined. Here the results for $M_\Gamma = 0{\cdot}3$ are presented for comparison. Figure 2(a) shows the results for $m = -5, 0, 5$. The axial component of the mean flow produces a Doppler shift in $\mathrm{Re}\,(k_{mn})$, so that all evanescent and amplifying modes will propagate only upstream. In a frame of reference moving with the local mean velocity, such modes do not propagate. For $m = 0$, the calculations show two propagating modes, and an infinite discrete set of evanescent and amplifying modes (the latter are usually discarded in applications as non-physical). For non-axisymmetric modes ($m \neq 0$), because of the Doppler effect due to the swirling component of the mean flow, there are more acoustic modes swirling in the direction opposite to the mean flow rotation. This results from the fact that for such modes the modified frequency $\tilde{\omega}_m$ is larger than ω, when m is negative. In addition to the discrete set of acoustic eigenvalues, a continuous spectrum of convected eigenvalues is seen from Figure 2(a). Note that for $m = 0$, there is a single convected eigenvalue.

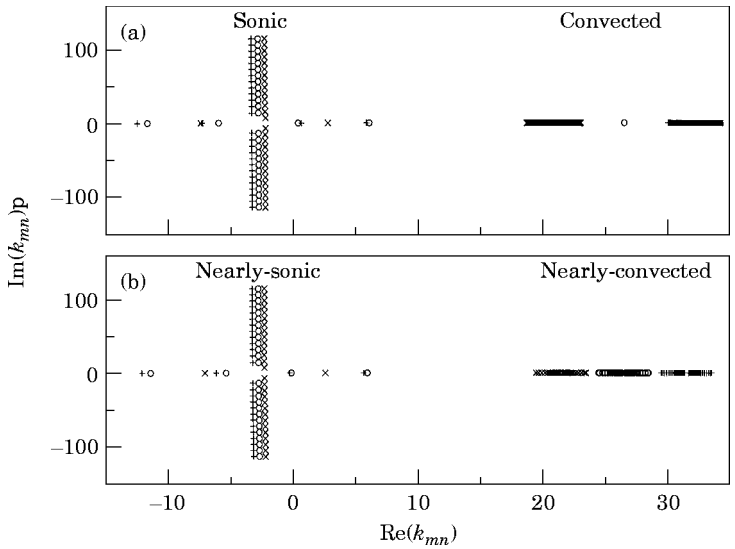

Figure 2. Eigenvalues $k_{mn}^{(u,d)}$ for $\bar{\omega} = 8$, $n = 1, \ldots, 15$: $+$, $m = -5$; $\bigcirc$, $m = 0$; $\times$, $m = 5$. (a) $M_0 = 0{\cdot}3$, $M_\Gamma = 0{\cdot}3$; (b) $M_0 = 0{\cdot}3$, $M_\Omega = 0{\cdot}3$.

Figure 2(b) shows the eigenvalues of equation (35) for the vortical flow with $M_\Omega = 0{\cdot}3$, $M_\Gamma = 0$, for modes with $m = -5, 0, 5$. Two *distinct* sets of eigenvalues are seen. The corresponding eigenmodes represent acoustic–vorticity waves. The acoustic–vorticity eigenmodes corresponding to the first set propagate with phase speeds close to the speed of sound, and will be *pressure-dominated*. Figure 3(a) illustrates the pressure and axial vorticity eigenmodes obtained from the normalized eigenvector in equation (36), for $m = 2$. The *vorticity-dominated* eigenmodes from the second set are shown in Figures 3(b, c).

Note that as k_{mn} gets closer to the critical value k_c, the modes exhibit oscillatory behavior with larger gradients. The set of *nearly-convected* eigenvalues contains two branches of eigenvalues which asymptotically (with increasing density) approach a singular point

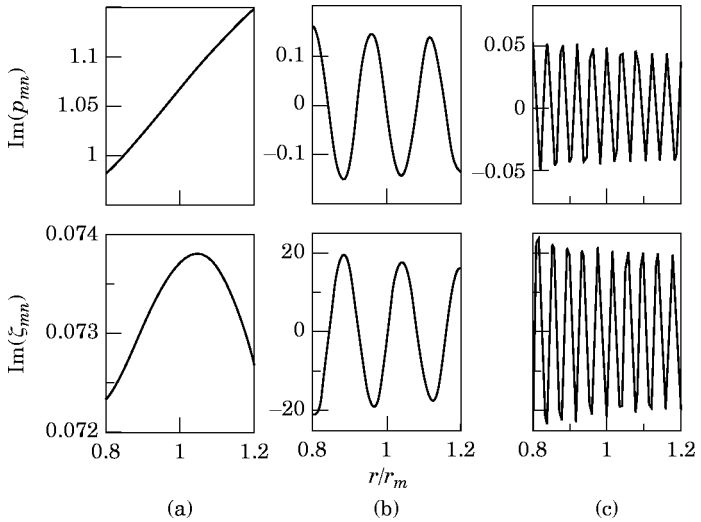

Figure 3. Pressure and axial vorticity eigenmodes for $M_0 = 0{\cdot}3$, $M_\Omega = 0{\cdot}3$, $\bar{\omega} = 8$, $m = 2$. Pressure dominated eigenmodes: (a) $k_{mn} = 5{\cdot}37$. Vorticity-dominated eigenmodes: (b) $k_{mn} = 23{\cdot}64$, (c) $k_{mn} = 24{\cdot}36$.

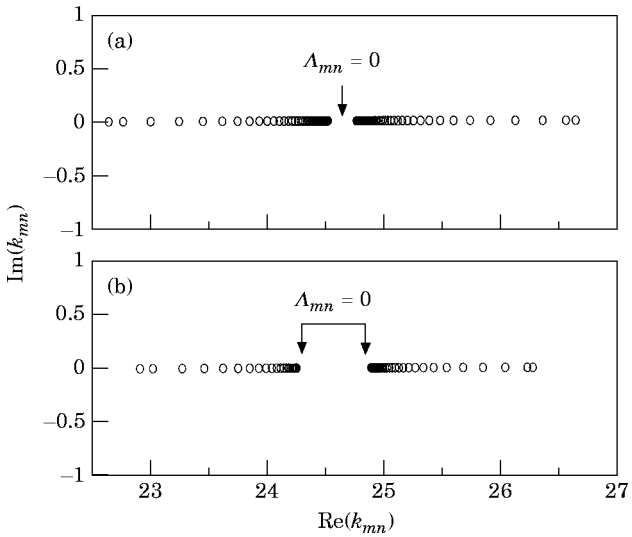

Figure 4. Nearly-convected eigenvalues for $\bar{\omega} = 8$, $m = 2$. (a) $M_0 = 0{\cdot}3$, $M_\Omega = 0{\cdot}3$. (b) $M_0 = 0{\cdot}3$, $M_\Omega = 0{\cdot}2$, $M_\Gamma = 0{\cdot}1$.

corresponding to a pure convection ($\Lambda_{mn} = 0$) (Figure 4(a)). As indicated before, these eigenvalues are located between the zeros of the polynomial $D(k_{mn}) = 0$ which appears in the coefficients of the eigenvalue equation (16). Therefore, it can be easily shown that

$$(\tilde{\omega}_m - 2\Omega)/U_0 \leqslant k_{mn} \leqslant (\tilde{\omega}_m + 2\Omega)/U_0. \tag{36}$$

The corresponding nearly-convected eigenmodes exhibit a sinusoidal behavior, with the frequency of oscillations increasing as the eigenvalues approach the critical point. Also, for such modes vorticity becomes more and more dominant (compare Figures 3(b) and 3(c)).

For a potential mean swirl, there is a continuous spectrum of convected eigenvalues, with the acting centrifugal forces giving rise to an algebraic growth of the corresponding vorticity modes [5, 8]. On the other hand, for a vortical mean swirl Coriolis forces deflect a perturbed fluid particle from its convected path, thus prohibiting a purely convected solution. This produces a mutual coupling of potential and vortical disturbances, which leads to a *critical layer* in the region of nearly-convected eigenvalues. This region is different depending on the nature of the swirl. Figure 4(b) shows details of the eigenvalues near the critical layer when the swirl contains both potential and vortical components, with $M_\Omega = 0{\cdot}2$ and $M_\Gamma = 0{\cdot}1$. The difference from the previous case (Figure 4(a)) results mainly from the fact that Λ_{mn} is now also a function of the radius. Therefore, the critical layer corresponding to a prohibited convected solution with $\Lambda_{mn}(k_{mn}, r) = 0$, now occurs for a range of eigenvalues $\tilde{\omega}_m(r_h)/U_0 \leqslant k_{mn} \leqslant \tilde{\omega}_m(r_t)/U_0$. Numerically, this range is filled with *spurious* roots which change their values depending on the number of collocation points in the numerical scheme. As one increases m from 2 to 20, the number of *physical* roots in the left and right branches gradually decreases, so that for $m = 20$ it reduces to one in each of the two branches (Figure 5). The set of nearly-convected eigenvalues is bounded by zeros of $D(k_{mn}, r) = 0$ so that

$$\frac{\tilde{\omega}_m(r_h) - 2\sqrt{\Omega(\Omega + \Gamma/r_h^2)}}{U_0} \leqslant k_{mn} \leqslant \frac{\tilde{\omega}_m(r_t) + 2\sqrt{\Omega(\Omega + \Gamma/r_t^2)}}{U_0}. \tag{37}$$

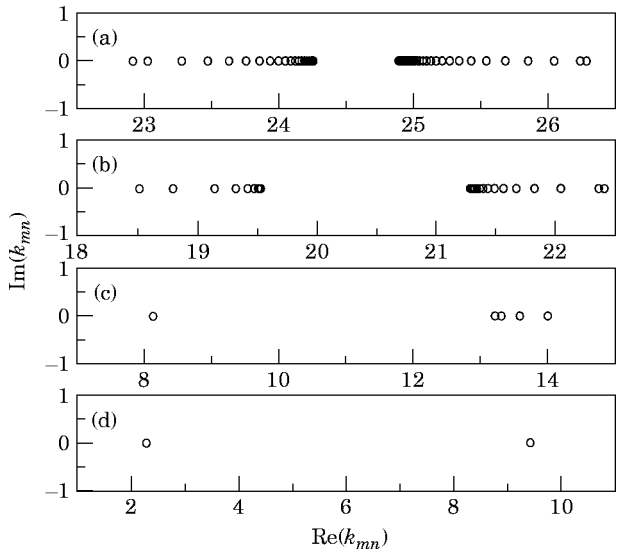

Figure 5. Numerical reduction of non-spurious roots for nearly-convected eigenvalues for $M_0 = 0{\cdot}3$, $M_\Omega = 0{\cdot}2$, $M_\Gamma = 0{\cdot}1$, $\bar{\omega} = 8$. (a) $m = 2$, (b) $m = 6$, (c) $m = 15$, (d) $m = 20$.

The behavior of nearly-convected eigenfunctions is shown for $m = 2$ in Figure 6. As one moves along the left branch of eigenvalues toward the left edge of the critical layer, the corresponding eigenfunctions become highly oscillatory near the hub radius (Figures 6(a, b)). A strong radial variation of amplitudes of the modes can also be noted. The same pattern, but near the tip radius, is observed for eigenmodes corresponding to the right branch of the eigenvalues (Figures 6(c, d)). Thus, as k_{mn} moves from the left to the right edge of the critical layer, the singularity travels from hub to tip radius. This singularity is related to the infinite peaks of the disturbance vorticity which occur at different radii depending on the mode wavelength. It may be worthwhile to state that this

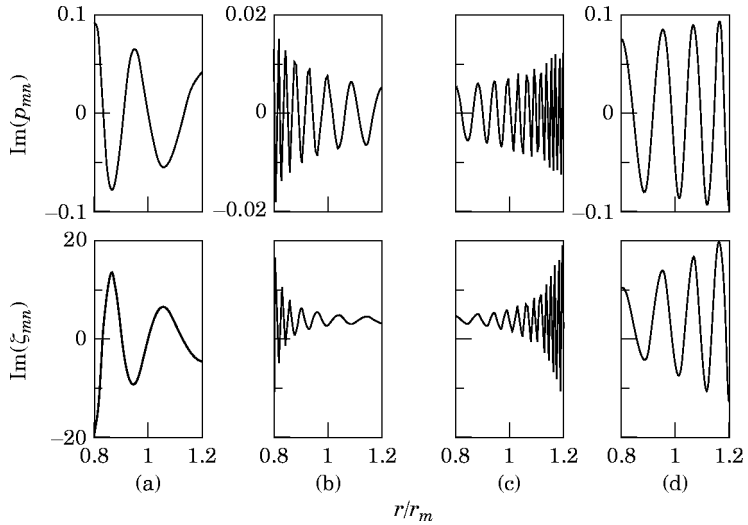

Figure 6. Nearly-convected pressure and axial vorticity eigenmodes for $M_0 = 0{\cdot}3$, $M_\Omega = 0{\cdot}2$, $M_\Gamma = 0{\cdot}1$, $\bar{\omega} = 8$, $m = 2$. (a) $k_{mn} = 23{\cdot}63$, (b) $k_{mn} = 24{\cdot}19$, (c) $k_{mn} = 24{\cdot}93$, (d) $k_{mn} = 25{\cdot}35$.

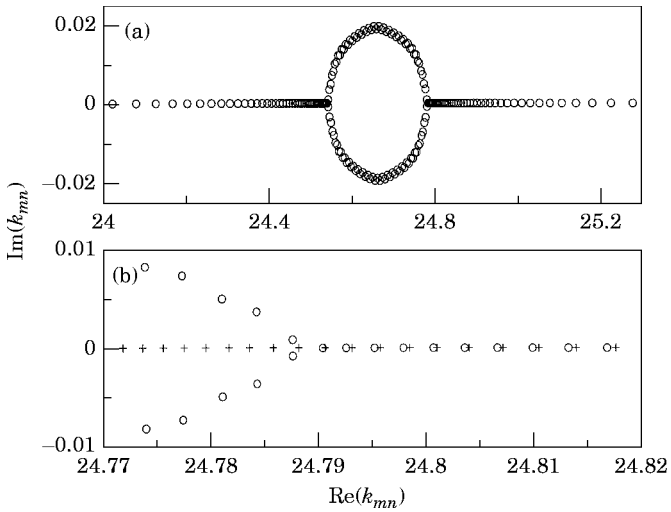

Figure 7. Nearly-convected eigenvalues for $M_0 = 0{\cdot}3$, $M_\Omega = 0{\cdot}3$, $\bar{\omega} = 8$, $m = 2$, $k_c = 24{\cdot}67$, ○, numerical solution; +, asymptotic solution. (a) Numerical results, (b) comparison of numerical and asymptotic solutions.

singular behavior is due to the omission of viscosity which must take care of dissipation of singular vorticity in the critical layer.

5. MULTIPLE-SCALE ANALYSIS OF THE CRITICAL LAYER

In the close vicinity of a critical layer, the results of numerical solution fail to accurately predict the behavior of nearly-convected modes. Figure 7(a) shows details of the nearly-convected eigenvalues from Figure 4(a), including the spurious roots for illustration. An asymptotic analysis is used to study the behavior of the eigenvalues and eigenfunctions for $\Lambda_{mn} \to 0$. Two cases of vortical mean swirl are considered separately as the corresponding asymptotic solutions show a remarkable distinction. The first case corresponds to a pure solid body rotation flow, and the second case represents a swirling flow composed of a solid body rotation and a free vortex. For convenience, all lengths in the present analysis are normalized by the mean radius of the annulus, r_m, and all velocities, by U_0.

5.1. SOLID BODY ROTATION MEAN SWIRL: $\Omega \neq 0$, $\Gamma = 0$.

To study the solution to the boundary-value problem (16, 17) one first introduces the fast variable, $\xi = (r - r_h)/\Lambda_{mn}$. It is convenient to introduce the critical eigenvalue $k_c = \omega_m = \omega - m\Omega$, which corresponds to $\Lambda_{nm} = 0$. It follows that $\Lambda_{mn} = k_{mn} - k_c$. Applying the stretching transformation $r \to \xi$ to equation (16), and keeping only the leading terms in Λ_{mn}, one obtains the simple eigenvalue problem,

$$\psi''_{mn\xi\xi} - (4m\Omega/r)\psi'_{mn\xi} + 4\Omega^2\{m^2/r^2 + k_{mn}^2\}\psi = 0 \tag{38}$$

with boundary conditions

$$\mathrm{d}\psi_{mn}/\mathrm{d}\xi = 0 \tag{39}$$

at $\xi_h = 0$ and $\xi = \xi_t = \Delta/\Lambda_{mn}(\Delta = r_t - r_h)$. The characteristic roots of equation (38) are

$$\gamma_{1,2}(k_{mn}) = 2m\Omega \pm 2\mathrm{i}\Omega k_{mn}, \tag{40}$$

and hence the eigenfunctions are of the form

$$\psi_{mn}(\xi) = A\exp(2m\Omega\xi)\cos(2\Omega k_{mn}\xi + \bar{\vartheta}, \tag{41}$$

where $\bar{\vartheta} = \tan^{-1}(m/k_{mn})$ and A is an arbitrary constant. Substituting equation (41) into conditions (39), one obtains the simple dispersion relation

$$2k_{mn}\Omega\xi_t = n\pi, \tag{42}$$

where n is an integer. This gives an infinite *discrete* spectrum of *real* eigenvalues,

$$k_{mn} = k_c \frac{\pi n U_0}{\pi n U_0 - 2\Omega\Delta}. \tag{43}$$

Since $|\Lambda_{mn}| = |\mathrm{k_{mn}} - k_c| \ll 1$, expression (43) is only valid for large positive and negative n. It is easy to see that as $n \to \pm\infty$, the eigenvalues cluster with increasing density approaching the critical layer (*accumulation* point):

$$\left|\frac{k_{mn} - k_c}{k_c}\right| \sim \frac{2\Omega\Delta}{n\pi} \tag{44}$$

The results of the multiple-scale analysis are compared with the numerical solution in Figure 7(b) which shows a blow-up of the right branch from Figure 7(a). These results compare well, but as k_{mn} approaches the critical point k_c, the numerical method fails to resolve the near singular behavior of the eigensolution. The numerical and asymptotic results start to diverge again farther away from the critical layer as Λ_{mn} increases and the asymptotic solution is no longer valid.

The eigenfunctions (41) expressed in terms of the slow variable, $r - r_h$, have the wavenumbers

$$\beta_{mn} \sim \pi n/\Delta \to \infty, \quad \text{as } n \to \infty. \tag{45}$$

This is in agreement with the highly oscillatory behavior of the nearly-convected modes throughout the annulus, $r_h \leqslant r \leqslant r_t$, found from the numerical analysis (see Figures 3(b)–(3)). Note that the wavenumbers (45) are independent of Ω.

Figure 8 shows a comparison between the normalzed values of ψ_{mn} obtained from the numerical calculations and the asymptotic results (41). The two results are in good agreement, thus validating the numerical approach.

5.2. GENERAL MEAN SWIRL: $\Omega \neq 0$, $\Gamma \neq 0$.

In the general case of a mean swirling flow with solid body rotation and free vortex, it is assumed that the parameters Ω and Γ have the same sign. This eliminates the possibility of hydrodynamic instability in the flow[1]. In particular, without loss of generality, it is assumed that $\Omega > 0$ and $\Gamma > 0$. Again, it is convenient to introduce the critical eigenvalue

$$k_c(r) = \tilde{\omega}_m(r) = \omega - m(\Omega + \Gamma/r^2) \tag{46}$$

which corresponds to $\Lambda_{mn} = 0$. Since Λ_{mn} vanishes for a range of r, a critical layer may exist for a range of values $k_{mn} = \mathrm{k_c}$. For modes spinning in the direction of the swirl, $m > 0$, this layer extends for

$$\tilde{\omega}_m(r_h) \leqslant k_c \leqslant \tilde{\omega}_m(r_t), \tag{47}$$

[1]Rayleigh's criterion for inviscid instability reduces for this flow to $\Omega(\Omega + \Gamma) < 0$.

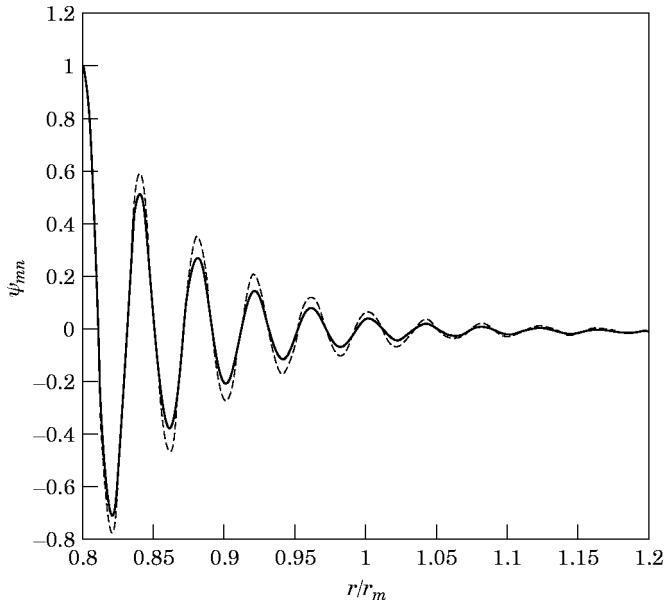

Figure 8. Comparison of numerical (——) and asymptotic (– – –) eigenfunctions ψ_{mn}, $M_0 = 0.3$, $M_\Omega = 0.3$, $\bar{\omega} = 8$, $m = 2$, $n = 20$, $k_{mn} = 24.36$.

and for those spinning in the opposite direction $m < 0$, for

$$\tilde{\omega}_m (r_t) \leqslant k_c \leqslant \tilde{\omega}_m (r_h) \tag{48}$$

Note that for an axisymmetric disturbance, $m = 0$, the critical layer collapses to a single point $k_c = \omega$, and the analysis becomes similar to the previous case of $\Gamma = 0$.

In order to develop an asymptotic analysis similar to Section 5.1 for eigensolutions near the critical layer, one assumes that $|\Lambda_{mn}| \ll 1$. The fast variable $\xi(r)$ is introduced by

$$d\xi = -dr/\Lambda_{mn}. \tag{49}$$

Note that, in general, Λ_{mn} may be complex.

Outside the critical layer,

$$\Lambda_{mn} = k_{mn} - k_c^b + m\Gamma \left(\frac{1}{r^2} - \frac{1}{r_c^2}\right), \tag{50}$$

where $\Lambda_{mn} (k_c^b, r_c) = 0$, and r_c can be the hub or the tip radius of the annulus. In what follows, $r_c = r_h$ is assumed. An asymptotic analysis of the behavior of the eigenvalues k_{mn} near the left border of the critical layer is derived for $m > 0$, i.e., $k_{mn} \to k_c^h$, where $k_c^h = \tilde{\omega}_m(r_h)$ (a similar analysis can be applied for $m < 0$).

Note that since asymptotic analysis assumes $|\Lambda_{nm}| \ll 1$ for the range of $r_h \leqslant r \leqslant r_t$, this requires that $(r_t - r_h)/r_m \ll 1$. Thus integrating equation (49) and keeping the leading terms, one obtains the expression for the fast variable,

$$\xi(r) = \frac{1}{2m\Gamma} \ln \left[1 - 2m\Gamma \frac{(r - r_h)}{(k_{mn} - k_c^h)}\right]. \tag{51}$$

Substituting equation (49) into equation (16) yields, to leading order,

$$\psi''_{mm\xi\xi} - 2m\,(2\Omega + \Gamma)\psi'_{mn\xi} + 4\Omega(\Omega + \Gamma)\{m^2 + k_{mn} = 0, \tag{52}$$

with the same wall conditions (39) at $\xi = \xi_h$ and $\xi = \xi_t$. Equation (52) has the characteristic roots:

$$\gamma_{1,2}(k_{mn}) = -m(2\Omega + \Gamma \pm [m^2\Gamma^2 - 4\Omega k_{mn}^2(\Omega + \Gamma)]^{1/2}. \tag{53}$$

and thus the eigenfunctions are

$$\psi_{mn}(\xi) = B \exp[-m(2\Omega + \Gamma)\xi] \cos(\tilde{\beta}_{mn}\xi + \bar{\phi}), \tag{54}$$

where $\tilde{\beta}_{mn} = [4\Omega k_{mn}^2(\Omega + \Gamma) - m^2\Gamma^2]^{1/2}$, $\bar{\phi} = \tan^{-1}[m(2\Omega + \Gamma)/\tilde{\beta}_{\mathrm{mn}}]$ and B is an arbitary constant. It is interesting to note the similarity between the eigensolution (54) and that obtained in Section 2.2.

Applying conditions (39) gives the following dispersion relation,

$$\tilde{\beta}_{\mathrm{mn}}\xi_{\mathrm{t}} = n\pi, \tag{55}$$

where $\xi_t = \xi(r_t)$, and n is a positive integer. Since $|k_{mn} - k_c^h| \ll 1$, one can expand $\tilde{\beta}_{mn}$ to obtain

$$\tilde{\beta}_{mn} = \sqrt{4\Omega(k_c^h)^2(\Omega + \Gamma) - m^2\Gamma^2}\,[1 + Q(k_{mn} - k_c^h)] + \ldots., \tag{56}$$

where

$$Q = 4\Omega k_c^h(\Omega + \Gamma)/a, \tag{57}$$

and $a = 4\Omega(k_c^h)^2(Q + \Gamma) - m^2\Gamma^2$. This shows that eigensolutions exist only for

$$m^2 < 4\Omega(k_c^h)^2(\Omega + \Gamma)/\Gamma^2 \tag{58}$$

which is the same condition obtain in the critical layer analysis in Section 2.2.

Substituting expressions (51) and (56) into equation (55) and equating the leading order terms gives

$$|k_{mn} - k_c^h| \sim 2m\Gamma\Delta \exp\{-2n\pi m\Gamma/\sqrt{a}\}. \tag{59}$$

This result shows that, while for the previous case of $\Omega \neq 0$, $\Gamma = 0$ the eigenvalues accumulate algebraically near the critical point as $n \to \infty$ (equation (44)), the eigenvalues will accumulate exponentially at the edge of the critical layer for the general swirl.

If one introduces $k_{mn} = \alpha_{mn} + i\kappa_{mn}$ and $k_{mn} - k_c^h = |k_{mn} - k_c^h|\exp(i\vartheta)$, and equates the leading order imaginary terms, then

$$\vartheta \sim -Q\,\kappa_{mn} \ln|k_{mn} - k_c^h|, \tag{60}$$

where

$$\vartheta = \tan^{-1}\frac{\kappa_{mn}}{\alpha_{mn} - k_c^h}. \tag{61}$$

If $\vartheta = O(1)$, then $\kappa_{mn} = O(1/n0$, but this is not acceptable in view of equation (59), hence $\vartheta \ll 1$. Equating equations (60) and (61) shows that κ_{nm} vanishes faster than $\exp\{-2\pi\pi m\Gamma/\sqrt{a}\}$, thus implying a real solution for k_{mn}.

It is easy to generalize this analysis for eigenvalues in the vicinity of both k_c^h and k_c^t,

$$|k_{mn} - k_c^h| \sim 2m\Gamma\Delta \exp\{-2|n|\pi m\Gamma/\sqrt{a}\}. \tag{62}$$

The asymptotic results ('+' symbol) are compared with those of the direct numerical solution of eigensystem (13) (in circles) in Figure 9. The enlargements of the left and right branches of the nearly-convected eigenvalues are shown for varying radial modal numbers n and a set of parameters $M_0 = 0.3$, $M_\Omega = 0.2$, $\mathrm{M}_\Gamma = 0.1$ and $\bar{\omega} = 8$ (as in Figure 4(b)). Note that the numerical solution is in good agreement with the asymptotic results except

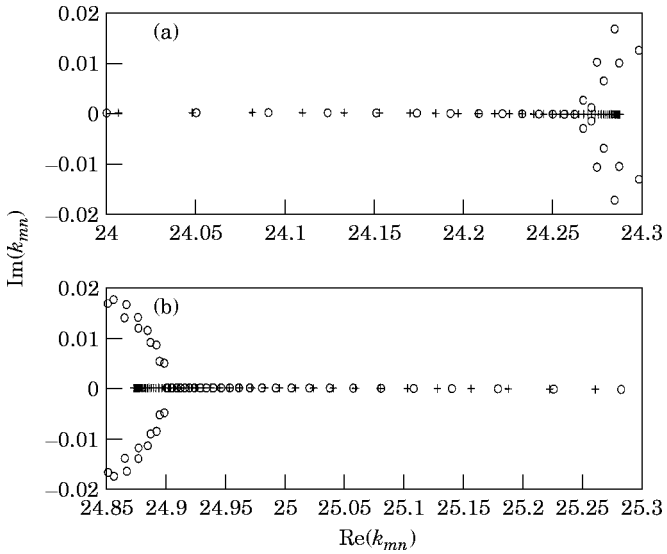

Figure 9. Comparison of numerical and asymptotic solutions for nearly-convected eigenvalues, $M_0 = 0.3$, $M_\Omega = 0.2$, $M_\Gamma = 0.1$, $\bar{\omega} = 8$, $m = 2$, $24.49 \leqslant k_c \leqslant 24.87$, $\bigcirc$, numerical solution, $+$, asymptotic solution. (a) Left and (b) right branch.

in the immediate vicinity of the borders of the citical layer. On the other hand, as the eigenvalues depart away from the critical layer, the asymptotic results may become a less accurate representation of the solution. These results also show the accuracy of the numerical procedure employing a pseudo-spectral method.

As it was indicated in the critical-layer analysis of Section 2.2, there are no oscillatory eigensolutions for $m^2 \geqslant 4\Omega k_c^2(\Omega + \Gamma)/\Gamma^2$. If

$$\Omega(\Omega + \Gamma)^3 > \Gamma^2/4. \tag{63}$$

there are no eigensolutions for the range of circumferential wavenumbers satisfying

$$\frac{\omega}{\Omega + \Gamma + \Gamma/[2\sqrt{\Omega(\Omega + \Gamma)}]} \leqslant m \leqslant \frac{\omega}{\Omega + \Gamma - \Gamma/[2\sqrt{\Omega(\Omega + \Gamma)}]} \tag{64}$$

On the other hand, if

$$\Omega(\Omega + \Gamma)^3 < \Gamma^2/4, \tag{65}$$

no eigensolutions will exist for

$$m \leqslant \frac{\omega}{\Omega + \Gamma - \Gamma/[2\sqrt{\Omega(\Omega + \Gamma)}]} \tag{66}$$

and

$$m \geqslant \frac{\omega}{\Omega + \Gamma + \Gamma/[2\sqrt{\Omega(\Omega + \Gamma)}]} \tag{67}$$

Therefore, for each mode m there will be a cut-off (*or* cut-on) frequency band of width

$$\delta\omega = m\Gamma/\sqrt{\Omega(\Omega + \Gamma)}. \tag{68}$$

Note that for $\Gamma = 0$, the eigensolutions will always exist in the vicinity of the critical point. The *cut-off* band (68) corresponding to condition (63) will increase as the portion of the potential swirl component increases for Ω-fixed and $\Gamma \to \infty$. On the other hand, if Γ is fixed and $\Omega \to 0$, condition (65) will hold and thus the *cut-on* band $\delta\omega \to \infty$. In this limit, the critical layer vanishes and the eigenvalues form a continuum convected spectrum.

For each m from the ranges (64), (66) and (67), a critical layer with $k_{mn} = k_c$ will occur at some radial position $r_h \leqslant r_c \leqslant r_t$. From expression (59), as m increases toward its cut-off values, the eigenvalues approach the edge of the critical layer faster. As a result, the direct numerical analysis fails to resolve the area of eigenvalues which concentrates too close to the critical layer, and this explains the results in Figure 5. To obtain the correct solution for m from the cut-off ranges, viscous dissipative effects will need to be included in the analysis.

6. CONCLUSIONS

The propagation of the acoustic–vorticity waves in an annular duct with mean swirling flow has been investigated. The mean flow is composed of a uniform flow, free vortex rotation, and rigid body rotation. The analysis shows that the disturbances can be split into a nearly-convected vorticity dominated part and a nearly-sonic pressure dominated part, obeying weakly coupled equations. The coupling between vorticity and pressure is due to Coriolis and centrifugal forces. The nearly-convected modes can be identified with the purely convected gusts in a non-swirling flow.

A normal mode analysis leads to a singular eigenvalue problem unless the mean swirl is potential. A pseudo-spectral method is used to calculate the eigenvalues and the corresponding eigensolutions. However, near the critical layer, an asymptotic analysis is developed to accurately resolve the solutions.

The results show two families of solutions. The first family comprises the pressure dominated modes which may propagate with different phase speeds both upstream and downstream. Due to the Doppler frequency shift most non-axisymmetric modes propagate opposite to the mean flow swirl. The second family represents vorticity dominated nearly-convected eigenmodes. These modes are split into two branches and clustered with increasing density as they approach the accumulation critical layer. The *continuous* spectrum of convected eigenvalues in the case of a potential swirl changes in the case of a vortical swirl to an infinite *discrete* spectrum of eigenvalues accumulating on either sides of the critical layer. The rate of accumulation appears to be different for a pure solid body rotation flow and a flow composed of a solid body rotation and a free vortex. When both the solid body and the free vortex induced rotations are in the same direction, no unstable nearly-convected modes have been found outside the critical layer.

ACKNOWLEDGMENTS

The research was supported by the Office of Naval Research Grant No. N00014-92-J-1165, and monitored by Mr L. Patrick Purtell, and NASA Lewis Research Center Grant No. NAG3-732, and monitored by Mr Dennis L. Huff. V. V. Golubev would like to thank the Center for Applied Mathematics at the University of Notre Dame for its support.

REFERENCES

1. H. M. Atassi 1994 *Aerodynamics and Aeroacoustics* (editor K.-Y. Fung, World Scientific) **IV**, 121–172. Unsteady aerodynamics of vortical flows: early and recent developments.
2. J. L. Kerrobrock 1977 *American Institute of Aeronautics and Astronautics Journal* **15**, 794–803. Small disturbances in turbomachine annuli with swirl.
3. D. W. Wundrow 1994 *Contractor Report* 195406, NASA. Small-amplitude disturbances in turbomachine flows with swirl.
4. J. H. Horlock 1958 *Axial Flow Compressors*. Butterworths Scientific Publications.

5. V. V. Golubev and H. M. Atassi 1996 *Journal of Sound and Vibration* **198**, 601–616. Sound propagation in an annular duct with mean potential swirling flow.
6. A. H. Nayfeh, J. E. Kaiser and D. P. Telionis 1975 *American Institute of Aeronautics and Astronautics Journal* **13**, 130–153. Aeroacoustics of aircraft engine-duct systems.
7. R. J. Briggs 1964 *Massachusetts Institute of Technology Research Monograph No*. 29. Electron-stream interaction with plasmas. Cambridge, Ma.: M.I.T. Press.
8. V. V. Golubev and H. M. Atassi 1995 *Proceedings of the First Joint CEAS/AIAA Aeroacoustics Conference*, Munich, Germany, June 12–15, 167–176. Aerodynamic and acoustic response of a blade row in unsteady swirling flow.
9. H.-C. Ku and D. Hatziavramidis 1984 *Journal of Computational Physics* **56**, 495–512. Chebyshev expansion methods for the solution of the extended Graetz problem.
10. W. H. Press, S. A. Teukolsky, W. T. Vetterling and B. P. Flannery 1988 *Numerical Recipes in FORTRAN*: *The Art of Scientific Computing*, Cambridge University Press.